JOURNAL OF AIRCRAFT
Vol. 60, No. 2, March–April 2023

Implementation of Multidisciplinary and Multifidelity Uncertainty Quantification Methods for Sonic Boom Prediction

Huseyin Emre Tekaslan,* Sihmehmet Yildiz,† Yusuf Demiroglu,‡ and Melike Nikbay§
Istanbul Technical University, Maslak, 34469 Istanbul, Türkiye

https://doi.org/10.2514/1.C036962

To advance a supersonic aircraft design process, an uncertainty quantification study is conducted for sonic boom prediction while considering uncertainties associated with flight and atmospheric conditions. The uncertainty quantification process is implemented within a multidisciplinary analyses framework and assisted with a multifidelity surrogate model based approach. The sonic boom prediction framework requires input from the flowfield pressure distribution solution to generate the near-field pressure signature of the aircraft, which is then propagated throughout the atmosphere to the ground by using aeroacoustic methods. The open-source SU2 suite is employed as a high-fidelity flow solver tool to obtain the aerodynamic solution, while in-house postprocessing scripts are developed to generate the required near-field pressure signature. For low-fidelity flow analysis, A502 PAN AIR, a higher-order panel code which solves flows around slender bodies in low angles of attack for subsonic and supersonic regimes, is used. For nonlinear aeroacoustic propagation, NASA Langley Research Center's code sBOOM exploits the near-field pressure signature for both high-fidelity and low-fidelity sonic boom calculations. Efficient uncertainty quantification tools are developed in house by implementing multifidelity polynomial chaos expansion and multifidelity Monte Carlo methods. Several flight and atmospheric parameters are selected to include randomness where these uncertainties are propagated into the sonic boom loudness prediction of the JAXA wing-body model, which is a low boom aircraft. Finally, an overall assessment of the multifidelity uncertainty quantification methods is presented in terms of efficiency and numerical accuracy.

Nomenclature

a_i	=	deterministic polynomial chaos expansion coefficients
$C_a(\theta_h)$	=	additive correction function
C_D	=	drag coefficient
C_L	=	lift coefficient
$C_m(\theta_h)$	=	multiplicative correction function
C_p	=	pressure coefficient
$\tilde{C}_a(\theta_h)$	=	polynomial chaos expansion based additive correction surrogate model
$\tilde{C}_m(\theta_h)$	=	polynomial chaos expansion based multiplicative correction surrogate model
d	=	order of polynomials
F_c	=	convective flux vector
$f_h(\theta_h)$	=	high-fidelity model response
$f_l(\theta_l)$	=	low-fidelity model response
$\tilde{f}_h(\theta_h)$	=	polynomial chaos expansion based high-fidelity surrogate model
$\tilde{f}_l(\theta_l)$	=	polynomial chaos expansion based low-fidelity surrogate model
H_d	=	Hermite polynomials with order of d
L	=	aircraft length
M_∞	=	freestream Mach number
m_i	=	number of evaluation of ith model
N	=	number of terms in total order expansion
N_h	=	number of high-fidelity samples
N_l	=	number of low-fidelity samples
n	=	number of random variables
P	=	pressure
p	=	total computational budget
R	=	radial distance between near-field signature location and aircraft axis
Q	=	conservative state vector
w_i	=	computational cost of ith model
$\mathcal{X}$	=	input domain
$\mathcal{Y}$	=	output domain
γ	=	correction weight
δ_{ij}	=	Kronecker delta function
ε_p	=	prediction error
ε_r	=	regression error
$\boldsymbol{\theta_h}$	=	high-fidelity input samples
$\boldsymbol{\theta_l}$	=	low-fidelity input samples
ξ	=	normalization operator
$\boldsymbol{\xi}$	=	normalized random variable vector
$\hat{\phi}$	=	perturbation velocity potential

I. Introduction

RELIABILITY and robustness requirements of aerospace engineering systems are of major importance and need to be assessed accurately and efficiently during the early phases of a design process to ameliorate certification tasks which are mandatory for the final design. Numerical assessment of system reliability and robustness is achieved through uncertainty quantification (UQ) methods that propagate the effect of uncertain variables to the overall system performance. If there are sufficient data about the distribution of the uncertainties pertaining to different random variables, probabilistic methods can be used for uncertainty quantification in a holistic approach. However, standard methods can be computationally costly as the number of uncertain variables increases. The abundance of uncertainties in aerospace engineering problems with extremely low allowances for failure reveals the need for implementation of more efficient and accurate multifidelity uncertainty propagation methods that can minimize the number of high-fidelity evaluations needed without sacrifice from the reliability. Therefore, this paper investigates the feasibility of multifidelity uncertainty modeling methods for a computationally expensive design problem in the context of sonic boom prediction for a supersonic aircraft.

Presented as Paper 2021-3100 at the AIAA Aviation Forum, Virtual, August 2–6, 2021; received 27 March 2022; revision received 8 July 2022; accepted for publication 29 September 2022; published online 14 December 2022.

*M.S. Student, Research Scholar, AeroMDO Lab, Faculty of Aeronautics and Astronautics. Student Member AIAA.

†Ph.D. Student, Research Assistant, AeroMDO Lab, Faculty of Aeronautics and Astronautics. Student Member AIAA.

‡M.S. Student, Research Assistant, AeroMDO Lab, Faculty of Aeronautics and Astronautics. Student Member AIAA.

§Professor, Faculty of Aeronautics and Astronautics, Astronautical Engineering Department; nikbay@itu.edu.tr. Associate Fellow AIAA.

A deterministic design approach falls to be insufficient when crossover design improvements for a supersonic aircraft need to be investigated, integrated, and certified based on the relevant sonic boom limitations over populated land. With a deterministic design perspective, the resulting sonic boom loudness may not always guarantee to comply with a predetermined threshold. For such tight design conditions, a supersonic aircraft noise would probably exceed the given threshold during flights in real-life conditions which exhibit a stochastic behavior. In this occasion, uncertainty quantification is a crucial procedure for supersonic aircraft design to ensure that the stochastic loudness level is always restrained below a certification value. Although reliable tools which solve for flow around a high-speed air vehicle and propagate acoustic waves through the atmosphere are sufficiently matured, those tools still lack the capacity of addressing inherent randomnesses within the design problem. In fact, over a million realizations may be required to propagate the probabilistic distributions and descriptive statistics of uncertain quantities of interest as a result of which computational burden becomes the leading impediment. As a remedy, surrogate models are favorable methods to reduce the expense of high-fidelity numerical solutions in uncertainty quantification processes. However, this computational expense can be further reduced by integrating several successful multifidelity methods into the surrogate models. The reduction in computational cost is accomplished by fusing a relatively large number of low-fidelity simulations with a few high-fidelity simulations. This feature increases the use of multifidelity methods in design optimization and uncertainty quantification studies.

Concerning uncertainty quantification for a low boom aircraft design, impact of aeroelastic uncertainties on sonic boom loudness were studied by Phillips and West [1] and Nikbay et al. [2]. In the context of multifidelity uncertainty quantification, West and Phillips [3] developed a polynomial chaos expansion based uncertainty quantification on sonic boom loudness with additive corrections and three levels of fidelity. In that work, time-dependent ground pressure signatures were not considered; however, we include them in this study. West and Gumbert [4] applied multifidelity polynomial chaos expansion to transonic airfoil and multidisciplinary aircraft design problems. Moreover, Wang et al. [5] inquired the efficacy of Gaussian process modeling in multifidelity uncertainty quantification via the polynomial chaos technique. Chaudhuri et al. [6] proposed a methodology for uncertainty quantification in multidisciplinary and coupled systems that reduced the required number of analyses by using adaptive surrogates. Additionally, Blonigan et al. [7] investigated an efficient uncertainty quantification framework with a combination of reduced-order models and sampling-based multifidelity methods. The multifidelity Monte Carlo (MFMC), which is a model management method, is preferred in studies with a high number of variables where it may be expensive to set up a surrogate model. The authors of [8] proposed a multifidelity approach for uncertainty quantification with Monte Carlo (MC) based on control variate variance reduction method that was applied to robust optimization of the acoustic horn. A study [9] addressed multifidelity uncertainty analysis for feedback-coupled blackbox problems with the help of adaptive surrogates which estimated coupling variables and adaptive sampling strategies. Impact of uncertain flow properties on an airfoil problem was investigated using multilevel MFMC in [10]. Peherstorfer et al. [11] developed an optimal model management algorithm for the MFMC method. Peherstorfer [12] used MFMC method with an adaptive low-fidelity model to obtain more accurate results with fewer data, and at the end of the study, the adaptive low-fidelity model based on the MFMC method was compared with the standard MFMC method. Additionally, Peherstorfer et al. [13] used the MFMC method for large-scale aerostructural uncertainty analysis and studied how the accuracy of the results changed depending on the combination of models with different correlation values. Blonigan et al. [7] proposed a sampling-based multifidelity approach that took Monte Carlo as the base.

The current study focuses on multifidelity uncertainty quantification with two-level fidelity methods for the sonic boom prediction. There are several studies in the literature using multifidelity methods to predict sonic boom signature [14–17]. Computational fluid dynamics (CFD) methods are widely used as high-fidelity methods, whereas panel methods are preferred as low-fidelity tools. In this regard, the open-source SU2 multiphysic suite [18] developed by Stanford University Aerospace Design Laboratory is implemented to our study as a high-fidelity solver for supersonic flow around the Japan Aerospace Exploration Agency (JAXA) Wing-Body model [14]. Besides, A502 PAN AIR code [19] is integrated into a multifidelity framework as a low-fidelity flow solver by virtue of supersonic flow solution capability. PAN AIR has been used as a low-fidelity prediction tool by researchers [14,15,20]. For aeroacoustics, NASA' sBOOM code [21] is implemented into the framework for both high- and low-fidelity analyses as a nonlinear sonic boom propagation method. A Python code is developed to couple sBOOM with SU2 and PAN AIR to facilitate the use in the multifidelity analysis framework. To the best of our knowledge, the most relevant work [3] was recently conducted using only multifidelity PCE with Cart3D and FUN3D flow solvers for NASA's commercial supersonic transport project. These solvers are officially released to NASA users, only. However, our work originates from a fully academic research project with limited resources and builds on open-source flow solvers and in-house academic codes to demonstrate an affordable multifidelity UQ approach for sonic boom loudness calculations. The only simulation tool that is not open-source in this framework is the public release (limited) version of the sBOOM code, which is licensed by NASA. On top of that, we demonstrate that multifidelity Monte Carlo method can be applicable to costly realistic engineering applications such as sonic boom UQ analysis. Eventually, a detailed comparison of the considered multifidelity UQ methods is provided, considering both analytical and sonic boom applications.

In this paper, we further implement multifidelity uncertainty quantification study for sonic boom loudness and ground pressure signature by employing multifidelity polynomial chaos expansion (MFPCE) and multifidelity Monte Carlo techniques. Section II introduces analytical derivations and implementation details about the near-field flow solutions, sonic boom predictions, and uncertainty quantification using multifidelity Monte Carlo and multifidelity polynomial chaos expansion methods as well as a computational test case. We present the sonic boom application and discuss the results and efficacy of the embraced methodology in Sec. III. Finally, a comprehensive assessment of the overall study is summarized in Sec. IV.

II. Methodology

In this section, we expound on the pursued methodology. First, high- and low-fidelity supersonic flow solutions, including acoustic propagation, are introduced. Then, analytical background for multifidelity uncertainty quantification methods are presented.

A. Near-Field Flow Solution

Accurate prediction of near-field pressure signature is essential for the sonic boom prediction. Therefore, CFD methods are widely used to predict the flowfield around an aircraft. In this study, the SU2 suite, developed by Standford University Aerospace Design Laboratory, is employed for the high-fidelity flow solution. For the current study, a steady inviscid compressible flow solution is performed with SU2. The governing equations of the high-fidelity solution are Euler equations as provided in Eq. (1) in differential form,

$$\frac{\partial Q}{\partial t} + \nabla \cdot \bar{F}_c(Q) = 0 \tag{1}$$

where Q is the conservative state vector, F_c is the convective flux vector, and t is time. Q and F_c are given by

$$Q = \begin{Bmatrix} \rho \\ \rho\bar{V} \\ \rho E \end{Bmatrix} \quad \bar{F}_c = \begin{Bmatrix} \rho\bar{V} \\ \rho\bar{V} \otimes \bar{V} + \bar{\bar{I}}p \\ \rho E\bar{V} + p\bar{V} \end{Bmatrix} \tag{2}$$

In Eq. (2), ρ, E, p, $\bar{V}$, and $\bar{I}$ represent density, energy per mass, thermodynamic pressure, velocity vector, and identity matrix,

respectively. A finite volume method with an edge-based data structure on a vertex-based dual grid is used in SU2. Weighted least-squares method is selected for the computation of spatial gradients for convective fluxes. Level-1 V cycle multigrid method is used.

The A502 code, known as PAN AIR, is employed in this study for the low-fidelity flow solutions. PAN AIR is a higher-order panel method program which solves the linearized potential flow equations. Because supersonic linearized flow can be solved by PAN AIR, it is preferred for low-fidelity solutions. The supersonic linearized method has two main assumptions: slender body and moderate angle of attack. Because low-boom aircraft models meet these requirements, PAN AIR is considered to be suitable for this study. The Prandtl–Glauert equation that is derived from small perturbation theory and irrotationality assumption is the governing equation of the linearized potential flow given by Eq. (3),

$$(1 - M_\infty^2)\hat{\phi}_{xx} + \hat{\phi}_{yy} + \hat{\phi}_{zz} = 0 \tag{3}$$

where subscripts x, y, and, z refer to Cartesian coordinates. The strengths of sources and doublets distributed over the aircraft surface are solved with the impermeability boundary condition in PAN AIR. Thus, PAN AIR calculates aerodynamic coefficients, surface pressure distribution, and in-flow C_p distribution by using these singularity strengths. Because a near-field pressure signature is required for the sonic boom analysis, the in-flow C_p distribution is linked with the sonic boom code via in-house scripts. However, because of the linear flow assumption, large oscillations are observed in the near-field pressure signature extracted from PAN AIR as explained in Sec. III.

B. Sonic Boom Prediction

The sBOOM code of NASA Langley Research Center is employed for the current study. The augmented Burgers equation is numerically solved in a ray tube coordinate system by using an operator splitting method with small step size [22]. These ray tube coordinates are calculated by geometrical acoustic methods. Some nonlinear propagation effects such as thermoviscous absorption and molecular relaxation are taken into account by the sBOOM solver. A nonlinear atmospheric acoustic solution in sBOOM takes significantly shorter time compared to the flow solution around an aircraft using SU2. Therefore, the nonlinear solution option in sBOOM is used for both high- and low-fidelity sonic boom predictions in this study.

To run the sBOOM code, near-field pressure signature and flight conditions such as Mach number and altitude must be introduced to the solver. As mentioned before, a near-field pressure signature can be provided from the flow solver. This signature must be computed at two to three body lengths away from the aircraft due to the acoustics solution assumption [21]. Then, sBOOM generates a ground pressure signature. Perceived loudness on the ground can be calculated from this ground pressure signature. Stevens's [23] Mark VII algorithm is widely used to calculate perceived loudness from pressure signature.

C. Multifidelity Nonintrusive Polynomial Chaos Expansion

The idea of homogeneous chaos was first introduced by Wiener [24] and has been widely used to incorporate randomness into deterministic models. The polynomial chaos expansion (PCE) method is a useful mathematical tool that leverages the orthogonality of polynomials to represent stochastic physical models with a convergent expansion. Besides, the nonintrusive version of PCE is used in this study to make the method suitable for blackbox engineering applications. Mathematically, a stochastic model is expressed with the input domain $\mathcal{X} \subseteq \mathbb{R}^n$ and the output domain $\mathcal{Y} \subseteq \mathbb{R}^m$ by defining a multivariate function $f(\boldsymbol{\theta}): \mathcal{X} \to \mathcal{Y}$, where $n, m \in \mathbb{Z}^+$ and $\boldsymbol{\theta} \in \mathcal{X}$. Then, the chaos expansion of a stochastic model that is a function of normally distributed random variables can be expressed as

$$f(\boldsymbol{\theta}) = a_0 H_0 + \sum_{i_1=1}^{\infty} a_{i_1} H_1(\xi_{i_1}(\boldsymbol{\theta})) + \sum_{i_1=1}^{\infty}\sum_{i_2=1}^{i_1} a_{i_1 i_2} H_2(\xi_{i_1}(\boldsymbol{\theta}), \xi_{i_2}(\boldsymbol{\theta})) + \sum_{i_1=1}^{\infty}\sum_{i_2=1}^{i_1}\sum_{i_3=1}^{i_2} a_{i_1 i_2 i_3} H_3(\xi_{i_1}(\boldsymbol{\theta}), \xi_{i_2}(\boldsymbol{\theta}), \xi_{i_3}(\boldsymbol{\theta})) + \ldots \tag{4}$$

In Eq. (4), H_d corresponds to the Hermite polynomials with the order of $d \in \mathbb{N}$ that are derived by using total order expansion for this study. Here, $a_i \in \mathbb{R}$ are deterministic coefficients that are obtained with L_2 sense in this study, and ξ is a normalization operator that maps input to the standard normal space and thus can be expressed as a function $\xi: \mathcal{X} \to \mathcal{N}(0, 1)$. In the following parts, $\boldsymbol{\xi} \in \mathbb{R}^n$ refers to normalized random variable vector, $\boldsymbol{\xi} \sim \mathcal{N}(0, 1)$. The purpose of using Hermite polynomials is that they are orthogonal to each other with respect to a normal distribution weight function $e^{-\xi^2/2}$ as given in Eq. (5),

$$\langle H_i(\boldsymbol{\xi}), H_j(\boldsymbol{\xi}) \rangle = \int H_i(\boldsymbol{\xi}) H_j(\boldsymbol{\xi}) e^{-(\xi^2/2)}\, \mathrm{d}\boldsymbol{\xi} = \delta_{ij} \tag{5}$$

where δ_{ij} is Kronecker delta. However, the Askey scheme [25] proposes other hypergeometric orthogonal polynomials contingent upon the distribution of random variables. Furthermore, the infinite expansion in Eq. (4) is truncated at a certain polynomial order in a way that it satisfactorily approximates the function $f(\boldsymbol{\theta})$. Generalization capability of the truncated expansion should be taken into consideration to balance exploration and exploitation of the surrogate model. The number of terms in the total order expansion N after truncation is determined by Eq. (6):

$$N = \frac{(n + d)!}{n!d!} \tag{6}$$

We adopt an oversampling ratio (OSR) of 2, which is the ratio of the response sampling size to the number of terms in the expansion as suggested by Hosder et al. [26] as a minimum OSR throughout this study.

We consider angle of attack, $\alpha \sim \mathcal{N}(\mu_\alpha, \sigma_\alpha^2)$, and Mach number, $\mathrm{M} \sim \mathcal{N}(\mu_\mathrm{M}, \sigma_\mathrm{M}^2)$, as normally distributed variables. On the other hand, reflection factor, $\kappa \sim \mathcal{U}(\kappa^l, \kappa^u)$, and ground elevation, $h_g \sim \mathcal{U}(h_g^l, h_g^u)$, are assumed to be uniformly distributed variables with a weight function of 1. Here, l and u superscripts, respectively, correspond to lower and upper bounds. As it is described in [27], matching the orthogonality of weighting functions and probability density functions improves the convergence and diminishes the nonlinearity of the polynomial expansion. Therefore, the reflection factor and ground elevation are incorporated into the expansion after a distribution transformation. Box–Muller transformation [28] is applied to map uniformly distributed data onto the normal distribution space in order to preserve orthogonality. However, a notable change in the model performance was not observed. Hence, we used mixed stochastic distributions together (i.e., uniform and normal distributions) in the polynomial expansion.

In this study, we implement MFPCE, proposed by [29], to propagate uncertainties within the sonic boom problem. The underlying principle of MFPCE is to ameliorate the low-fidelity PCE model with additive and multiplicative correction PCE models. We let input samples of high-fidelity simulations with sampling size N_h be $\boldsymbol{\theta}_h \in \mathbb{R}^{n \times N_h}$ and input samples of low-fidelity simulations with sampling size N_l be $\boldsymbol{\theta}_l \in \mathbb{R}^{n \times N_l}$, such that $N_h \ll N_l$. In this study, sampling is performed in a such way that the high-fidelity samples are a subset of the low-fidelity samples. Thus, the multifidelity correction surrogates are obtained with an improved accuracy. Otherwise, low-fidelity predictions should be calculated using the low-fidelity surrogate model exactly on the high-fidelity sample points to construct the correction models. Because using low-fidelity predictions will be less accurate than high-fidelity solver data, this reduces the accuracy of the correction surrogate models.

The crucial point in sampling is that input samples of high-fidelity analyses must be a subset of input samples of low-fidelity analyses,

$\boldsymbol{\theta}_h \subset \boldsymbol{\theta}_l$. This requirement can be directly satisfied with Halton sampling [30] by choosing different sampling sizes.

The correction PCE models are built on the discrepancy between high-fidelity [$f_h(\boldsymbol{\theta}_h)$] and low-fidelity [$f_l(\boldsymbol{\theta}_l)$], model responses. Basically, additive and multiplicative correction functions, respectively, shift and scale the low-fidelity response. Let additive and multiplicative correction functions be $C_a(\boldsymbol{\theta}_h): \mathcal{X} \to \mathcal{Y}$ and $C_m(\boldsymbol{\theta}_h): \mathcal{X} \to \mathcal{Y}$, respectively,

$$C_a(\boldsymbol{\theta}_h) = f_h(\boldsymbol{\theta}_h) - f_l(\boldsymbol{\theta}_h) \tag{7}$$

$$C_m(\boldsymbol{\theta}_h) = \frac{f_h(\boldsymbol{\theta}_h)}{f_l(\boldsymbol{\theta}_h)} \tag{8}$$

The defined correction functions given in Eqs. (7) and (8) are then used to build PCE-based correction surrogate models. Therefore, the MFPCE model can be constructed with a combination of these correction PCE models to approximate high-fidelity response:

$$\tilde{f}_{mf}(\boldsymbol{\theta}_h, \boldsymbol{\theta}_l) = \gamma[\tilde{f}_l(\boldsymbol{\theta}_l) + \tilde{C}_a(\boldsymbol{\theta}_h)] + (1-\gamma)\tilde{f}_l(\boldsymbol{\theta}_l)\tilde{C}_m(\boldsymbol{\theta}_h) \tag{9}$$

In Eq. (9), symbol $\sim$ is used to refer PCE-based surrogate models; $\tilde{f}_{mf}(\boldsymbol{\theta}_h, \boldsymbol{\theta}_l)$, $\tilde{f}_l(\boldsymbol{\theta}_l)$, $\tilde{C}_a(\boldsymbol{\theta}_h)$, and $\tilde{C}_m(\boldsymbol{\theta}_h)$ denote multifidelity, low-fidelity, additive, and multiplicative surrogate models, respectively. Additionally, $\gamma \in [0, 1]$ is defined to weight additive and multiplicative corrections. The authors of [29] proposed an expression for γ that minimizes the norm of correction surrogates as in Eq. (10):

$$\gamma = \frac{\langle \tilde{C}_m^2(\boldsymbol{\theta}_h) \rangle}{\langle \tilde{C}_m^2(\boldsymbol{\theta}_h) \rangle + \langle \tilde{C}_a^2(\boldsymbol{\theta}_h) \rangle} \tag{10}$$

D. Multifidelity Monte Carlo

The MFMC method combines the outputs of low- and high-fidelity models to calculate the statistical properties of the output distribution of the high-fidelity model for uncertain variables with a certain input distribution with significantly reduced cost. In typical multifidelity applications, few high-fidelity analyses are used to reduce the computational cost, where majority of the analyses are performed using low-fidelity analyses. In MFMC applications, a large number of low-fidelity analysis results are used to reduce the variance of the multifidelity prediction, whereas a small number of high-fidelity analyses are used for the unbiasedness of the prediction [13]. The MFMC method is essentially similar to the multilevel Monte Carlo method but uses a different procedure for combining models [31].

In definition, the high-fidelity model is denoted by $f^{(1)}$, whereas the low-fidelity models are denoted by $f^{(2)}, f^{(3)}, \ldots, f^{(k)}$, respectively, according to the level of fidelity. All models map from the input domain $\mathcal{X}$ to the same output domain $\mathcal{Y}$ ($f^{(i)}: \mathcal{X} \to \mathcal{Y}$). Calculation of the MFMC estimate is done within a certain calculation budget p. Therefore, the number of evaluations of the models and the cost of each model should be defined. In the formulation, the cost of the ith model and the number of evaluations are shown as w_i ($w_i > 0$ for $i = 1, .., k$) and m_i, respectively. The number of model evaluations is defined as $0 < m_1 \leq m_2 \leq \ldots \leq m_k$, which means that the high-fidelity model must be evaluated at least once, and the model is evaluated more as the model fidelity decreases.

The mean and variance of the $f^{(i)}$ model at the m_i realization point $(x_1, x_2, \ldots, x_{m_i})$ are calculated by the Monte Carlo method as in Eq. (11) and expressed as $\bar{y}_{m_i}^{(i)}$ and $\hat{V}_{m_i}^{(i)}$, respectively,

$$\bar{y}_{m_i}^{(i)} = \frac{1}{m_i}\sum_{j=1}^{m_i} f^{(i)}(x_j) \qquad \hat{V}_{m_i}^{(i)} = \frac{1}{m_i}\sum_{j=1}^{m_i}\left(f^{(i)}(x_j) - \bar{y}_{m_i}^{(i)}\right)^2 \tag{11}$$

In the MFMC method, the Monte Carlo estimators are combined to obtain the mean and variance of the multifidelity model as in Eqs. (12) and (13). In these equations, $\bar{y}_{m_i}^{(i)}$ and $\hat{V}_{m_i}^{(i)}$ are calculated using all realization points of the model $f^{(i)}$, whereas the $\bar{y}_{m_{i-1}}^{(i)}$ and $\hat{V}_{m_i-1}^{(i)}$ are calculated using the first m_{i-1} realization points of the model $f^{(i)}$:

$$\bar{y}^{MF} = \bar{y}_{m_1}^{(1)} + \sum_{i=2}^{k}\beta_i\left(\bar{y}_{m_i}^{(i)} - \bar{y}_{m_{i-1}}^{(i)}\right) \tag{12}$$

$$\hat{V}^{\mathrm{MF}} = \hat{V}_{m_1}^{(1)} + \sum_{i=2}^{k}\beta_i\left(\hat{V}_{m_i}^{(i)} - \hat{V}_{m_{i-1}}^{(i)}\right) \tag{13}$$

The MFMC estimator depends on the $\beta_2, \ldots, \beta_k$ coefficients and the number of model evaluations $m_1, m_2, \ldots, m_k$, and these parameters must be obtained in order to obtain the MFMC estimation. References [11,32] worked to determine the optimum β and m parameters. On the basis of these studies, these parameters are determined to minimize the variance value of the MFMC mean estimator given in Eq. (14) at the determined MFMC estimator budget p:

$$\mathrm{Var}[\bar{y}^{MF}] = \frac{(\sigma_{m_1}^{(1)})^2}{m_1} + \sum_{i=2}^{k}\left(\frac{1}{m_{i-1}} - \frac{1}{m_i}\right)\left(\beta_i^2(\sigma_{m_i}^{(i)})^2 - 2\beta_i\rho_{1,i}\sigma_{m_1}^{(1)}\sigma_{m_i}^{(i)}\right) \tag{14}$$

In this equation, $\sigma_{m_i}^{(i)}$ shows the standard deviation of the ith model at the m_i realization point, and $\rho_{1,i}$ shows the correlation coefficient between the ith model and the high-fidelity model. The MFMC estimator cost is obtained as in Eq. (15):

$$c(\bar{y}^{MF}) = \sum_{i=1}^{k} w_i m_i = \boldsymbol{w}^T\boldsymbol{m} \tag{15}$$

Using Eqs. (14) and (15), the optimization problem needed to find the optimum values of the β and m parameters required for MFMC estimation can be written as in Eq. (16):

$$\begin{aligned} \underset{m\in\mathbb{R}^k,\beta_2,\ldots,\beta_k\in\mathbb{R}}{\arg\min} \quad & J(\boldsymbol{m}, \beta_2, \ldots, \beta_k) = Var[\bar{y}^{MF}] \\ \text{subject to} \quad & m_{i-1} - m_i \leq 0, \qquad i = 2, \ldots, k \\ & -m_1 \leq 0, \\ & \boldsymbol{w}^T\boldsymbol{m} = p \end{aligned} \tag{16}$$

Optimum β and m values are obtained by solving the optimization problem. Using the optimum parameters, the MFMC estimates are obtained through Eqs. (12) and (13).

E. Computational Test Case: Borehole Function

First, an uncertainty quantification study is performed on an analytical function to validate the in-house codes and compare their performance in different dimensional problems. The Borehole equation, used to validate multifidelity surrogate modeling codes in the literature [33], is implemented as a benchmark equation in this study. High-fidelity (HF) and low-fidelity (LF) Borehole functions are depicted in Eqs. (17) and (18), respectively. The MFMC method basically calculates the number of HF and LF analyzes to be used by referring to the correlation coefficient between the two models. Therefore, because the correlation between the original LF and HF Borehole equations is high, a uniformly varying noise parameter, $\eta \sim \mathcal{U}(-1, 1)$, is added to the LF equation to reduce the correlation:

$$f_{HF}(x) = \frac{2\pi T_u(H_u - H_l)}{\ell_n(r/r_w)(1 + (2LT_u)/(\ell_n(r/r_w)r_w^2K_w) + (T_u/T_l))} \tag{17}$$

Table 1 Statistics of random variables

Variable	Statistics
r_w	$\mathcal{U} \sim (0.05, 0.15)$
r	$\mathcal{U} \sim (100, 5000)$
T_u	$\mathcal{U} \sim (63700, 115600)$
H_u	$\mathcal{U} \sim (990, 1100)$
T_l	$\mathcal{U} \sim (63.1, 116)$
H_l	$\mathcal{U} \sim (700, 820)$
L	$\mathcal{U} \sim (1120, 1680)$
K_w	$\mathcal{U} \sim (9855, 12045)$

$$f_{LF}(x) = \frac{5T_u(H_u - H_l)}{\ell_n(r/r_w)(1.5 + (2LT_u)/(\ell_n(r/r_w)r_w^2K_w) + (T_u/T_l))} + \eta \tag{18}$$

The distribution of random variables used in the uncertainty quantification is shown in Table 1.

Uncertainty analysis is performed using the MFMC and MFPCE methods. Using the MC results, the developed codes are validated and compared for an eight-dimensional benchmark problem.

1. *Uncertainty Quantification with Multifidelity Monte Carlo*

The MFMC method decides on the number of LF and HF analyses to be used within a certain budget by referring to the correlation value between the models. Therefore, it is necessary to determine the budgets of the computations, and in this application, the LF and HF analysis costs were accepted as 0.5 and 1, respectively. Using these cost values, MFMC estimates are made for different computational budgets.

The MFMC mean and variance estimates with respect to the computational budget are, respectively, depicted in Figs. 1 and 2. As MF estimation with a low computational budget is made using few high-fidelity analyses, mean and variance estimations have a high error rate. Unlike the PCE surrogate models, the MFMC calculations are performed through a stochastic process that requires optimization of hyperparameters. In the MFMC method, the correlation calculation between fidelities and MF estimates depends on the selected samples. Therefore, to make a consistent comparison between the methods, the MFMC study should be repeated at least three times for different budget values, and the result should be presented. In this study, 100 repetitions were easily performed for each budget value because the models are composed of only analytical equations. The mean values of the results obtained at the end of each replication are shown with the red line in the graph, and the minimum and maximum

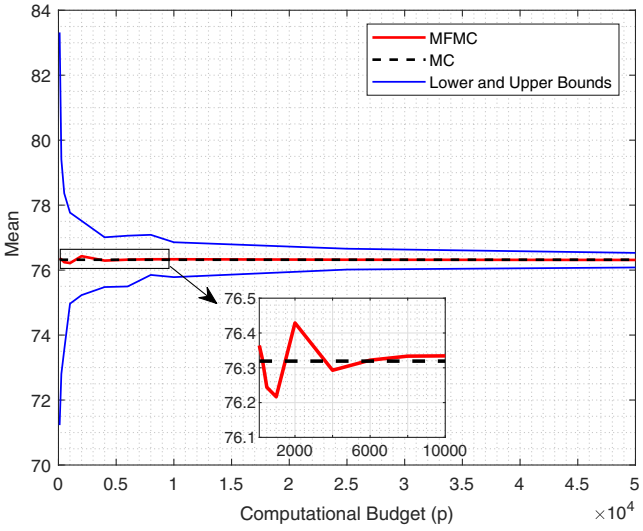

Fig. 1 MFMC mean estimation based on changing budget.

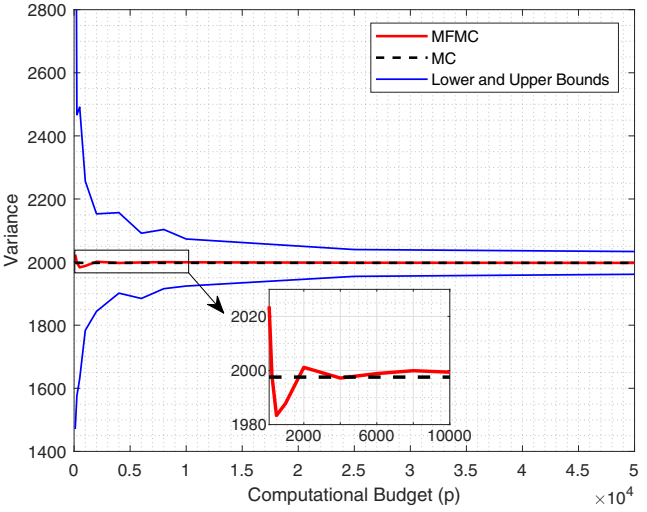

Fig. 2 MFMC variance estimation based on changing budget.

values of the results obtained in the replications are shown with the blue lines in the graph. As shown in Figs. 1 and 2, as the number of analyses increases due to the budget increase, the amount of changes in the results decrease. The MFMC method gives closer results to the MC results with fewer high-fidelity analysis results.

As can be seen from the results in Table 2, the MFMC method gives results close to the MC method with a small number of HF analysis results. However, the reliability of the results increases as the budget increases. Computation times of the MFMC method are given in the table, and the values are the duration of 100 iterations for each budget. It can be seen from the results that uncertainty quantification results can be obtained in less than 1 s for the eight-dimension problem.

2. *Uncertainty Quantification with Multifidelity Polynomial Chaos Expansion*

Polynomial chaos expansion is known for its weakness in high-dimensional problems as the number of terms within the expansion dramatically increases according to Eq. (6). In this computational experiment, we investigate how PCE performs in the presence of a high number of variables and compare with MFMC in terms of accuracy and computational cost. Because MFMC yields the mean and variance based on a budget value, comparison is done with a MFMC budget of 10,000, which corresponds 224 high-fidelity and 19,550 low-fidelity model responses. As the number of low-fidelity analyses is adequate, a PCE-based surrogate model on low-fidelity data is trained and tested up to the polynomial order of 8 to observe computation time. Regression and prediction errors and computational time are, respectively, depicted in Figs. 3 and 4. According to Fig. 3, the surrogate model tends to overfit after the polynomial order of 4. Thus, the fourth-order LF–PCE surrogate is used in the multifidelity part of this section. Additionally, the computational time steeply rises with the increasing polynomial order. Not only does computational time get heavier, but the memory usage also does; however, this can be mitigated with efficient matrix operations, which are not included in the scope of this paper.

Furthermore, regression and prediction errors of the correction surrogates follow a trend similar to the low-fidelity surrogate model errors, which are depicted in Fig. 3. The lowest prediction error of additive correction surrogate model on the test data is obtained as 6.1×10^{-3} using the polynomial order of 2. Meanwhile, third-order PCE is used for a multiplicative correction surrogate with the lowest prediction error of 3.1×10^{-3}. Besides, UQ is carried out with 10^5 realizations by using the multifidelity model; besides, results are compared with the evaluation of Eqs. (17) and (18) at sampled realizations. Efficacy of correction functions is also examined by constructing the MFPCE surrogate with different correction functions. Acquired distributions from all fidelity levels are given as histogram in Fig. 5. Distributions demonstrate that MFPCE satisfactorily keeps up with the trend of the high-fidelity function; nevertheless, discrepancies on account of

Table 2 The number of analyses used and MFMC estimates based on budget

Budget p	100	500	1000	2000	4000	10,000	25,000	50,000	MC
Number of HF model evaluation	2	11	22	44	89	224	562	1124	1e+7
Number of LF model evaluation	195	977	1955	3910	7820	19550	48875	97750	— —
Mean	76.3641	76.2441	76.2167	76.4289	76.2929	76.3242	76.3127	76.3197	76.3192
Standard deviation	44.9858	44.5347	44.5853	44.7344	44.6900	44.7144	44.6984	44.6927	44.6680
Model training and evaluation time, s	0.127	0.149	0.163	0.185	0.212	0.476	0.902	1.622	1.042

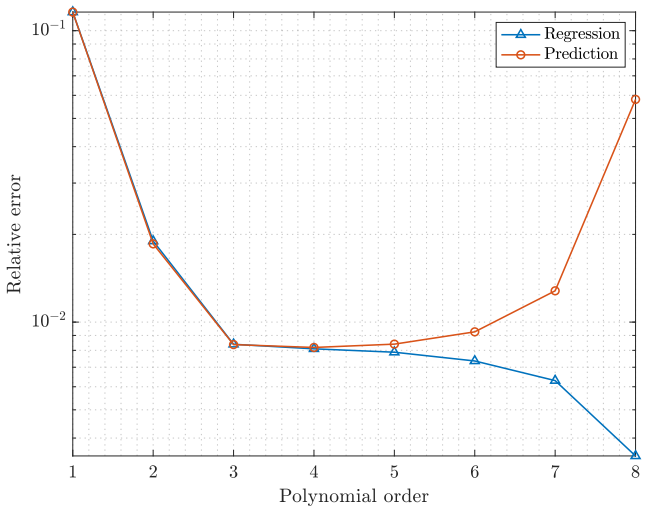

Fig. 3 Regression and prediction errors of the LF PCE.

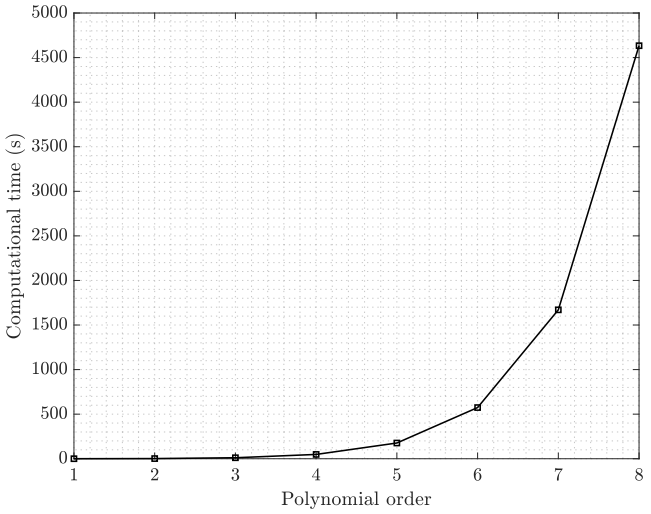

Fig. 4 Computational time of training and test of LF PCE.

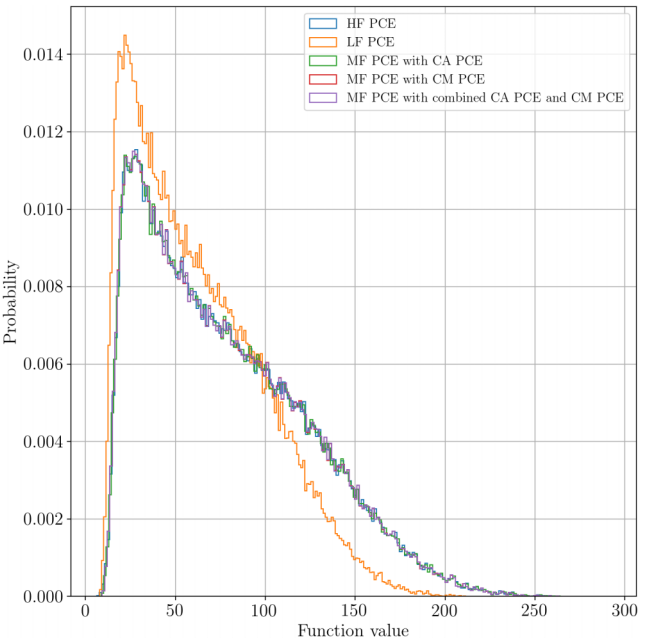

Fig. 5 Comparison of probability distributions from different fidelity levels.

Table 3 Comparison of MFMC and MFPCE in the application of Borehole function

Method	Mean	Standard deviation	Computation time, s
HF MC	76.3095	44.7121	— —
MFMC ($p = 10000$)	76.3242	44.7144	0.476
MFPCE Additive correction	76.3056	44.6765	92.247
MFPCE Multiplicative correction	76.3082	44.6900	103.604
MFPCE Additive + Multiplicative correction	76.3078	44.6877	109.218

correction functions are negligible. Descriptive statistics and computation times of both MFMC and MFPCE are tabulated in Table 3 for the convenience of the reader. As Table 3 reveals, all methods give reasonable descriptive statistics; however, MFMC is the fastest method by far.

III. Application

This section introduces multifidelity uncertainty quantification techniques applied to sonic boom prediction of a supersonic wing–body configuration called the JAXA Wing-Body (JWB) model by considering randomnesses in atmospheric and flight conditions. Within this framework, the angle of attack, Mach number, atmospheric reflection factor, and ground elevation are considered to possess uncertainties. The JWB model is introduced, and sonic boom computations are presented with the validation results for the JWB model. Finally, the uncertainty quantification techniques and multifidelity methods implemented into the current sonic boom prediction framework are elaborated.

A. JAXA Wing-Body Case Description

A multifidelity modeling based uncertainty quantification study is conducted for a low-boom supersonic aircraft by implementing the multifidelity Monte Carlo and multifidelity polynomial chaos expansion techniques. Because of the possible limitations of the low-fidelity analysis model, a wing–body combination is preferred rather than a full realistic aircraft model. Therefore, the JWB model is used as a functional geometry for the uncertainty quantification study. The JWB model was designed by JAXA for the Second AIAA Sonic Boom Prediction Workshop to provide the same equivalent area distribution as the NASA C25D aircraft [34]. In the following section, high- and low-fidelity analyses and the sonic boom prediction model are explained for the cruise conditions. For the uncertainty quantification study, four random variables, which are Mach number, angle of attack, ground elevation, and atmospheric reflection factor are chosen because these variables can vary instantly during the real flight.

1. Analysis Setup

The open-source multiphysics simulation and design software SU2 is employed for the high-fidelity flow solutions. To maintain an affordable number of elements in the grid structure due to the computational limits, inviscid analyses are executed with steady compressible Euler equations. The Mach number of all the analyses is set as 1.6, which is the design Mach number for the JWB model. The Jameson–Schmidt–Turkel scheme is chosen for the calculation of the convective fluxes where the flow domain is discretized into 12.8 million elements without using adaptive mesh refinement. An unstructured mesh is generated in the close neighborhood of the aircraft, while the remaining part of the solution domain is discretized with Mach-aligned prisms. For the convergence criteria in the analyses, the root mean square of the density value is set to 10^{-7}. Even though this convergence value is relatively high for the sonic boom predictions, it is adequate for the uncertainty quantification and optimization studies. A near-field pressure signature comparison is also provided in the following section.

For the low-fidelity analyses, PAN AIR is employed in this study. PAN AIR has the capability of supersonic potential flow solution with the assumptions of slender body and moderate angles of attack. Because the JWB model is a convenient case for these assumptions, it can be modeled in PAN AIR. The JWB analysis using PAN AIR was presented in detail by Carpenter et al. [15]. In the current study, a pressure distribution very close to the Euler analysis is obtained on the surface, except for the tail of the body. Here, 4000 quadrilateral elements are discretized on the surface to be used in PAN AIR. The maximum number of elements allowed by the current version of PAN AIR has been selected. A wake region is generated, starting from the trailing edge of the wing and base edges of the body. Structured discretization of the JWB surface is illustrated in Fig. 6.

Sonic boom prediction is performed by using NASA's sBOOM code; sBOOM requires a near-field pressure signature and input file containing parameters that define sonic boom analysis. In a previous study [16], the Python wrapper developed in Istanbul Technical University (ITU) Aerospace Multidisciplinary Design Optimization (AeroMDO) Laboratory to run sBOOM with SU2 and PAN AIR was presented. Therefore, this in-house code is implemented in the current study. The near-field pressure signature is computed at two body lengths away from the aircraft. Reflection factor and ground elevation are considered as random variables. The standard atmosphere profile is selected, and flight altitude is input as 52,000 ft with a Mach number of 1.6.

Next, a Python code is developed to automate the analysis procedure to generate a data set for both high- and low-fidelity solutions. First, this code reads a text file containing random variables. Then, it calls the flow analysis programs to generate a near-field pressure signature. Next, the Python wrapper for the sBOOM code is run based on the near-field pressure signature and random variables such as the reflection factor and ground elevation. The ground signature from sBOOM is used to calculate the loudness value with Utah State University (USU) Aero Laboratory's PyLdB code [35]. Finally, the obtained results are written to a text file to be used in the uncertainty analysis.

2. Results of Sonic Boom Analyses

An Euler analysis using the SU2 code is performed on a workstation which has 2.4 GHz processors with 36 cores and 192 GB RAM. Solution converged for the root mean square of density with 566 iterations in 65 min. Mach number distribution on the symmetry plane is depicted in Fig. 7.

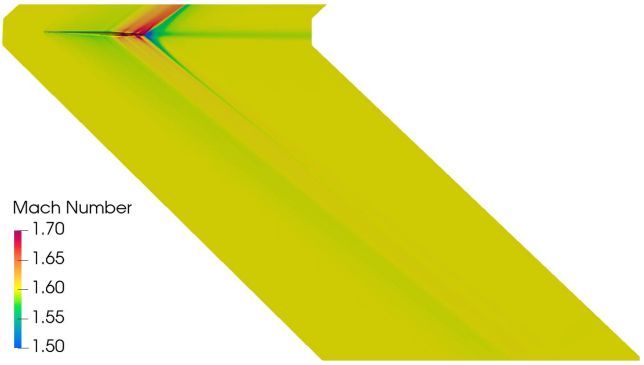

Fig. 7 Mach number distribution on the symmetry plane (high fidelity).

PAN AIR analysis takes approximately 15 min on a single core with supersonic solid surface boundary condition, which is approximately 100 times faster than an SU2 analysis that takes 65 min on 36 cores. For this reason, considering these real-time costs, the costs of high- and low-fidelity solvers are determined as 1 and 0.01 unit budgets, respectively. Surface pressure coefficient distribution is illustrated in Fig. 8 and compared with the SU2 results for both upper and lower surfaces of the aircraft.

In the PAN AIR analysis, some fluctuations in the near-field pressure signature are observed near the tail region of the body. These fluctuations occur due to the assumption of potential flow in PAN AIR. A comparison for the near-field pressure signature and ground signature, taken at $R/L = 3$, is exhibited in Figs. 9 and 10, respectively. Because the pressure signature in [34] is provided at $R/L = 3$, validation study is performed at three body lengths, while the two body lengths signal location is preferred for the UQ study to reduce the computational cost. Large spikes form in the near-field signature of the PAN AIR solution as expected due to low-fidelity analysis assumptions. Also, the near-field pressure signatures are compared with [34], and the ground signatures are compared with [15] for validation.

Table 4 shows the aerodynamic coefficients and loudness value of both high- and low-fidelity solutions in Perceived Loudness dB (PLdB). Also, the differences between the two fidelity levels are provided The difference in loudness value is due to the large fluctuations in the low-fidelity near-field pressure signature.

To quantify an error related to mesh dependence in high-fidelity solver, a mesh convergence study is performed with four different mesh structures using the SU2 CFD solver. The resultant values are provided in Table 5. Because of the limit of computational power, a mesh grid with approximately 12.8 elements is preferred in the UQ study.

B. Multifidelity Uncertainty Quantification of Sonic Boom Loudness

Uncertainty of sonic boom loudness level is investigated using the MFPCE and MFMC methods. The angle of attack, Mach number,

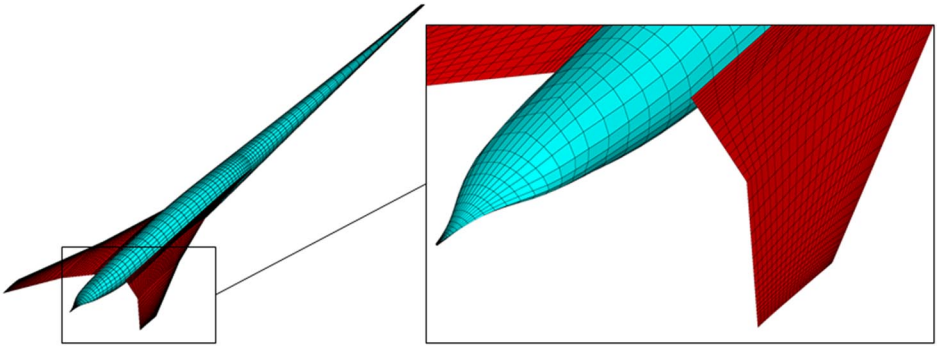

Fig. 6 Surface discretization of the JWB model.

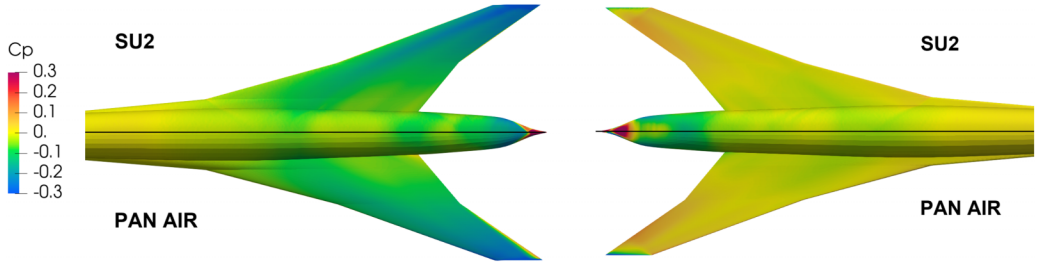

a) C_p distribution on the upper surface b) C_p distribution on the lower surface

Fig. 8 Pressure coefficient distribution comparison on the surface, PAN AIR and SU2.

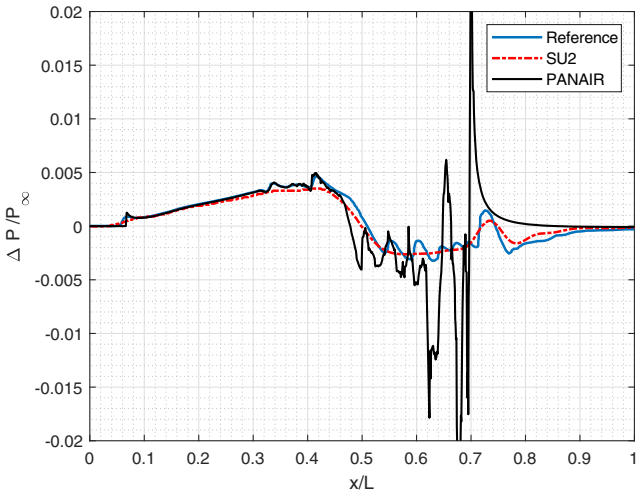

Fig. 9 Near-field pressure signatures for the JWB model.

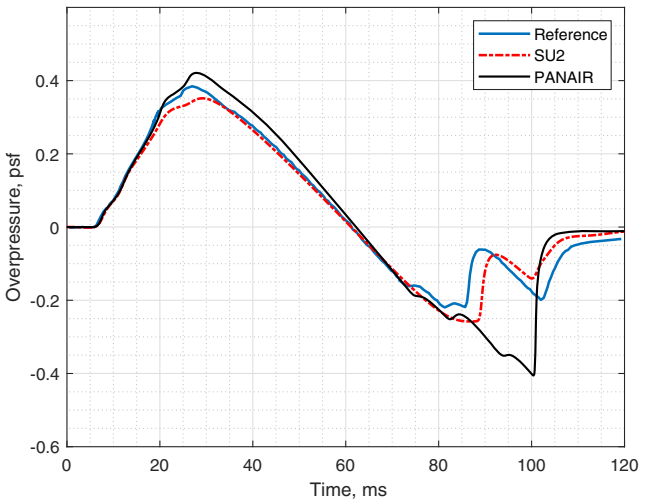

Fig. 10 Ground signatures for the JWB model.

Table 4 Aerodynamic coefficients and loudness values obtained with PAN AIR and SU2 for the JWB model

Solvers	C_L	C_D	Loudness, PLdB
SU2	0.07785	0.00708	77.40508
PAN AIR	0.07227	0.00641	87.08112
Difference	0.00558	0.00067	−9.67604

Table 5 Aerodynamic coefficients and loudness values for different meshes

Mesh size (million elements)	Solution time, min	C_L	C_D	Loudness, PLdB
7.33	101.1	0.077798	0.007082	76.44
12.81	171.9	0.077845	0.007083	77.41
16.78	267.9	0.077832	0.00708	78.32
22.98	335.8	0.077853	0.007081	78.48

Table 6 Statistics of random variables

Variable	Statistics
Angle of attack, deg	$\mathcal{N} \sim (3.07, 0.1^2)$
Mach	$\mathcal{N} \sim (1.6, 0.0016^2)$
Reflection factor	$\mathcal{U} \sim (1.8, 2)$
Ground elevation, ft	$\mathcal{U} \sim (0, 5000)$

reflection factor, and ground elevation are incorporated into the computation of loudness as random variables. Statistics of these variables are listed in Table 6. Standard deviation values of normally distributed random variables are selected as in [36].

1. Uncertainty Quantification with Multifidelity Polynomial Chaos Expansion

To obtain multifidelity model that we plan to propagate uncertainties with, model exploration is performed for each surrogate model to select the best model in terms of prediction. Both low-fidelity and high-fidelity data sets are split into training and test sets with 80–20 weights. We measure the regression and prediction accuracies of each model by using training and test data sets, respectively. Therefore, surrogate models are built by using the training data sets, only. The regression accuracy of each model is evaluated based on a relative error, and we define a general error function as in Eq. (19):

$$\varepsilon_r = \frac{\|f_{\text{in}}(\boldsymbol{\xi}) - \tilde{f}(\boldsymbol{\xi})\|_F}{\|f_{\text{in}}(\boldsymbol{\xi})\|_F} \tag{19}$$

Here, $f_{\text{in}}(\boldsymbol{\xi})$ is the training data on which surrogates are constructed, and $\tilde{f}(\boldsymbol{\xi})$ denotes the surrogate model prediction of training data set. On the other hand, we expect each surrogate model to estimate a test data set within an acceptable error margin. Thus, we measure the prediction accuracy of each model as given in Eq. (20) similar to the regression accuracy:

$$\varepsilon_p = \frac{\|f_{\text{out}}(\boldsymbol{\xi}) - \tilde{f}(\boldsymbol{\xi})\|_F}{\|f_{\text{out}}(\boldsymbol{\xi})\|_F} \tag{20}$$

Now, $f_{\text{out}}(\boldsymbol{\xi})$ is the test data. Additionally, model exploration is performed up to a polynomial expansion degree of 5 using the sonic boom loudness data. Results are depicted in Fig. 11. Triangular

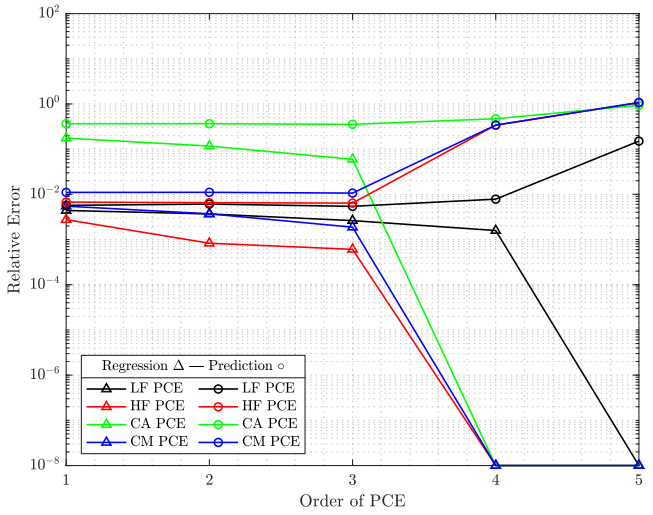

Fig. 11 Model exploration results of surrogate models.

Table 7 Model exploration results of surrogate models

Surrogate model	Errors	Order of PCE 1	2	3	4	5
LF PCE	ε_r	0.00235	0.00179	0.00141	0.00079	≈0
	ε_p	0.00270	0.00265	0.00253	0.00276	0.15344
HF PCE	ε_r	0.00276	0.000829	0.000607	≈0	≈0
	ε_p	0.00674	0.00654	0.00640	0.33933	1.07224
CA PCE	ε_r	0.05032	0.02036	0.010831	≈0	≈0
	ε_p	0.07347	0.07153	0.08195	0.30806	1.06071
CM PCE	ε_r	0.00453	0.00174	0.00095	≈0	≈0
	ε_p	0.00675	0.00658	0.00746	0.33870	1.07440

markers (Δ) refer to the regression errors, whereas circular markers (∘) correspond to the prediction errors. Error values are also tabulated in Table 7, in which CA PCE and CM PCE denote PCE-based approximates of additive correction and multiplicative correction functions, respectively.

PCE orders that give the lowest prediction errors are taken as a basis to construct the onward surrogate models. Hence, third-order low- and high-fidelity and second-order additive and multiplicative correction PCE-based surrogates are built. The reason for the construction of HF PCE is to validate and compare MFPCE predictions at the end of the study. In addition, all models meet the minimum OSR requirement of 2. Higher-order expansion is not preferred for all models to avoid overfitting, which may lead to biased estimation. It is experienced that fifth- and higher-order polynomial regressions bring about nonphysical estimations due to the loss of generalization (i.e., overfitting). Eventually, the MFPCE model is built by using Eq. (9).

One million realizations are generated for each random variable with the statistics given in Table 6. Uniformly distributed angle of attack and Mach number samples are transformed into normal distribution by using Box–Muller transformation; however, resulting distributions and descriptive statistics do not significantly change. Afterward, Hermite polynomials are evaluated at realizations to compute decibel levels. The entire process including random sampling, construction of surrogates, and uncertainty quantification is completed in 18.87 s with a 2.3 GHz dual-core processor. Loudness distributions yielded by uncertainty quantification on low-, high-, and multifidelity surrogate models and their box plots are demonstrated in Figs. 12 and 13, respectively.

Descriptive statistics are compared in Table 8. Results show that the MFPCE model can agreeably estimate descriptive statistics of sonic boom loudness level.

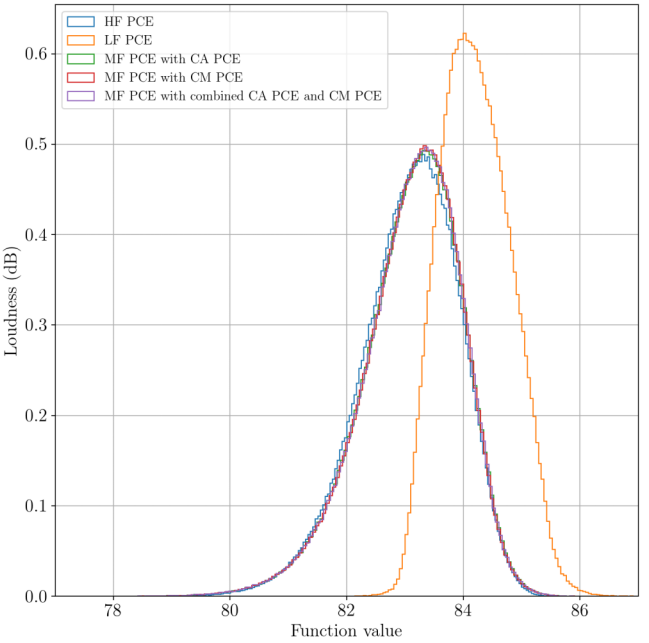

Fig. 12 Probability distributions of sonic boom loudness based on LF, HF, and MF surrogate models.

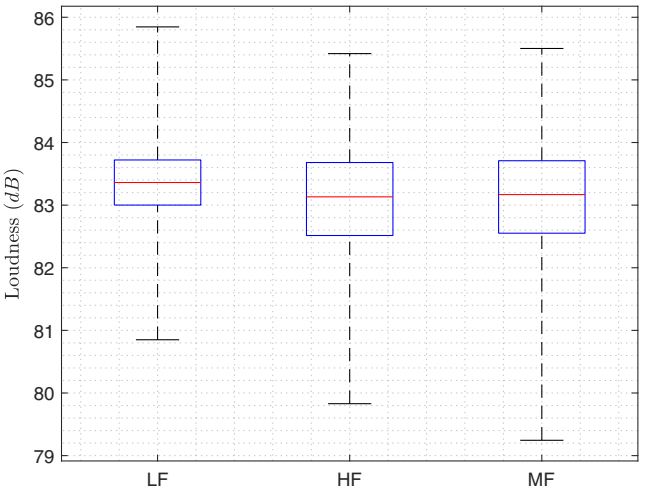

Fig. 13 Box plots of sonic boom loudness based on LF, HF, and MF surrogate models.

Table 8 Comparison of descriptive statistics of sonic boom loudness

Surrogate model	Mean, PLdB	Standard deviation, PLdB	Computation time, s
Low fidelity	83.3606	0.5350	— —
High fidelity	83.0702	0.8475	— —
Multi fidelity	83.1612	0.8495	4.032

2. Uncertainty Quantification with Multifidelity Monte Carlo

For the MFMC estimation, the number of model evaluations m and the β coefficients of the models should be calculated so as to minimize Eq. (14) within the determined budget p. For the budget constraint in the optimization problem defined in Eq. (14), first of all, it is necessary to determine the relative costs of low- and high-fidelity analyses. Because of the high number of realizations required in the MC method, in general, the MC method cannot be directly used with costly analysis programs in the process of UQ. As a remedy, we implement PCE-based surrogate models with the low- and high-fidelity data sets, separately to represent high- and low-fidelity solvers. To be in line with the previous modeling approaches, the

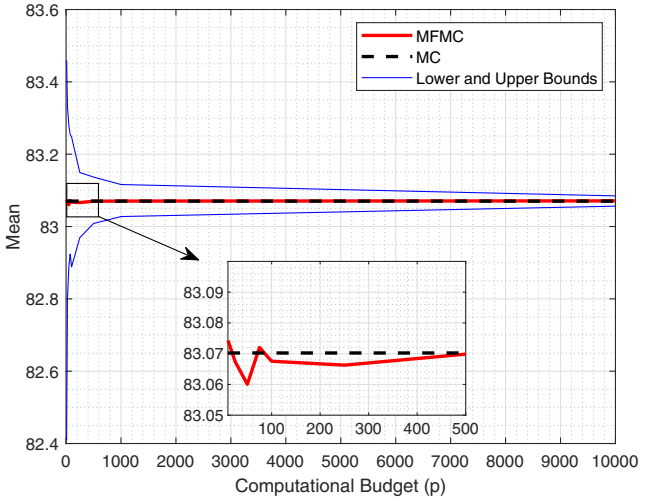

Fig. 14 MFMC mean estimation based on changing budget.

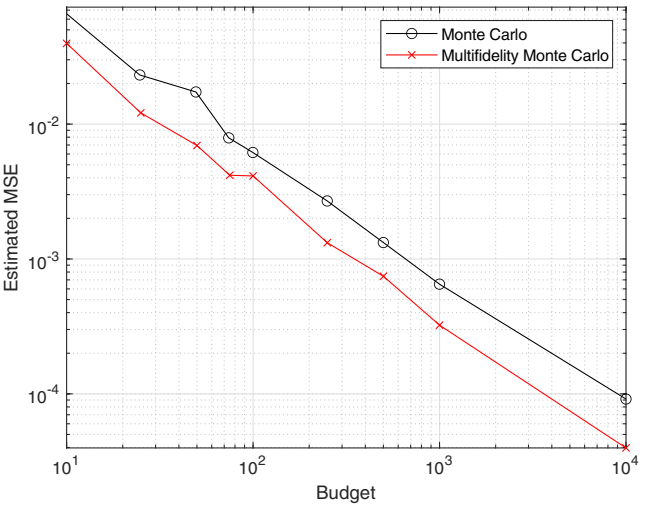

Fig. 16 MSE comparison of MFMC estimator (MSE = Mean squared error).

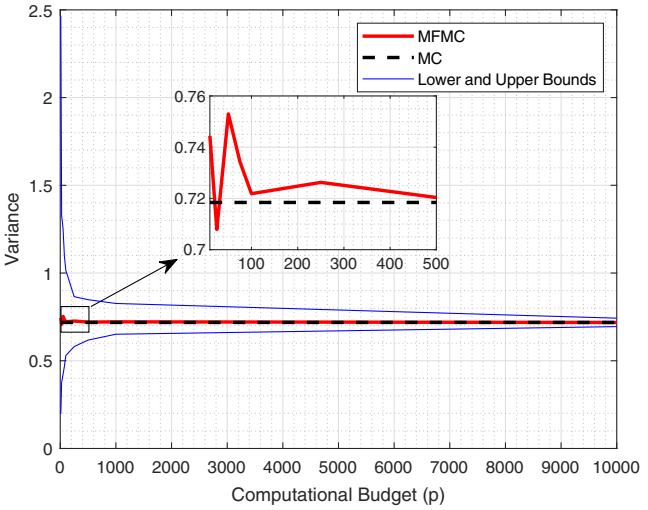

Fig. 15 MFMC variance estimation based on changing budget.

costs of running high- and low-fidelity PCE-based surrogate models are assumed to be 1 and 0.01 budgets, relatively. However, this is not exact in real time. Using these relative cost values, MFMC estimates of mean and variance are calculated as the calculation budget is increased from 10 to 10,000 units. Model evaluation numbers are determined by the optimization problem defined in Eq. (14) for certain budget values.

As a function of the calculation budget, the MFMC estimation of mean and variance are, respectively, demonstrated in Figs. 14 and 15. Because MF estimation with low computational budgets is made using a small number of high-fidelity analyses, the mean and variance values oscillate within a certain range depending on the input parameters of the HF samples. For this reason, multifidelity simulations are executed 100 times for each computational budget to make the most accurate MFMC predictions using the PCE-based surrogate models. The mean values of the results obtained at the end of each replication are shown with the red line in the graph, and the minimum and maximum values of the results obtained in the replications are shown with the blue lines in the graph. As Figs. 14 and 15 indicate, the amount of change in the results decreases with the increase in the number of analyses due to the budget increase, and the MFMC method gives results closer to the MC results. In general, with the budget exceeding 500 for this problem, the deviations in the mean and variance decrease and the results converge to the MC results calculated with 10^7 samplings.

MFMC estimates for different budget values are depicted in Table 9, and as can be seen from the results, the method gives results close to the MC results with a small number of HF analysis results. However, more reliable results are obtained with the increasing number of analyses due to the increase in the budget. The sum of the time for the establishment of the surrogate model and the realization of uncertainty quantification are presented in Table 9. It is seen that uncertainty quantification results can be obtained in 10–15 s.

To compare the MFMC method with the MC method (only HF simulation results), the mean estimation was made with the MC method using only high-fidelity analyses used at certain budget values. Estimated MSE values of the obtained results were calculated by accepting the results obtained with 10^7 sampling as the exact results. The results are shared in Fig. 16. Because the relative calculation cost of the high-fidelity analysis program is 1, the budget value represents the number of high-fidelity analyses used in the mean estimation of the MC method. The high- and low-fidelity analysis numbers used in the MFMC method are given in Table 9. As can be seen in Fig. 16, the MFMC method gives more accurate results with a small number of high-fidelity analyses in a fixed computational budget.

C. Multifidelity Uncertainty Quantification of Ground Pressure Signature

The prediction capability of the MFPCE-based reduced-order model on a scalar variable (i.e., sonic boom loudness in this study) is demonstrated in Sec. III.B. To investigate the performance of the MFPCE-based surrogates on a sequence of data, ground pressure signature estimation is performed. The ground pressure signature data set consists of time and overpressure values for different flow conditions. However, solutions do not share the same time axis even

Table 9 The number of analyses used and MFMC estimates based on budget

Budget p	10	25	50	75	100	250	500	1000	MC
Number of HF model evaluation	8	21	43	64	86	215	430	861	1e+7
Number of LF model evaluation	138	347	694	1041	1389	3473	6946	13893	— —
Mean, PLdB	83.0743	83.0674	83.0600	83.0720	83.0675	83.0663	83.0699	83.0704	83.0702
Standard Deviation, PLdB	0.8628	0.8414	0.8678	0.8569	0.8496	0.8522	0.8487	0.8485	0.8475
Model training and evaluation time, s	1.287	1.761	1.939	3.910	6.841	7.650	8.045	15.960	4.710

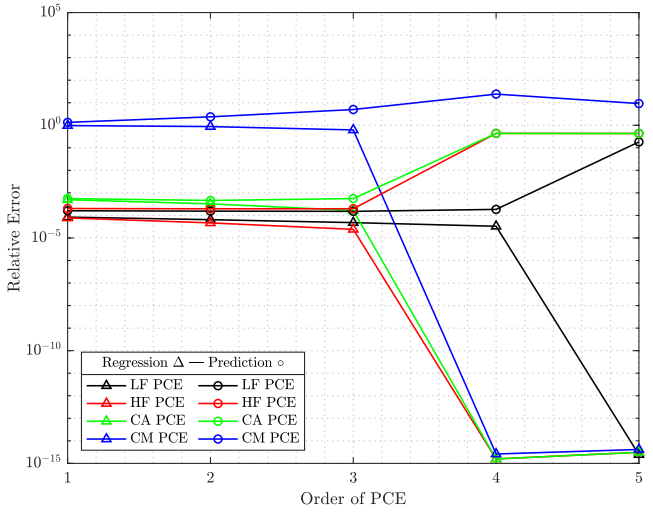

Fig. 17 Model exploration results of surrogate models in ground pressure signature prediction.

though they are quite close. This is because sBOOM does not produce the ground pressure signatures at the same time axis for each of the cases. Therefore, the obtained overpressure values have different time intervals. For instance, one of the ground pressure signatures takes 163.57 ms, while another one lasts 163.90 ms. This brings about variations in the time between two consecutive overpressure values. Thus, the time samples are varying from case to case; in other words, time is not definite. Because surrogate models are trained such that they predict both time and its corresponding overpressure value. Briefly, a similar methodology is followed as in the sonic boom loudness prediction. Model exploration results are depicted in Fig. 17. The error values are shown in Table 10.

The multiplicative correction surrogate model yields both the regression and prediction errors high as given in Table 10. Because the prediction error of the multiplicative correction model is high, the low-fidelity model is corrected by solely using the additive correction. The third-order LF PCE and second-order additive correction models are combined to obtain MFPCE.

A subset of random samples with a sampling size of 10^5 could not be propagated due to RAM restrictions. The entire process including the construction of surrogates and uncertainty quantification is

Table 10 Error values of surrogate models in ground pressure signature prediction

		Order of PCE				
Surrogate model	Errors	1	2	3	4	5
LF PCE	ε_r	8.43×10^{-5}	6.47×10^{-5}	4.79×10^{-5}	3.31×10^{-5}	≈0
	ε_p	0.00016	0.000155	0.000152	0.000190	0.18230
HF PCE	ε_r	7.74×10^{-5}	4.67×10^{-5}	2.41×10^{-5}	≈0	≈0
	ε_p	0.00674	0.00654	0.00640	0.33933	1.07224
CA PCE	ε_r	0.00050	0.00033	0.00017	≈0	≈0
	ε_p	0.00056	0.00046	0.00056	0.43645	0.43235
CM PCE	ε_r	0.96876	0.87466	0.62023	≈0	≈0
	ε_p	1.34403	2.36494	4.99396	24.14869	9.19023

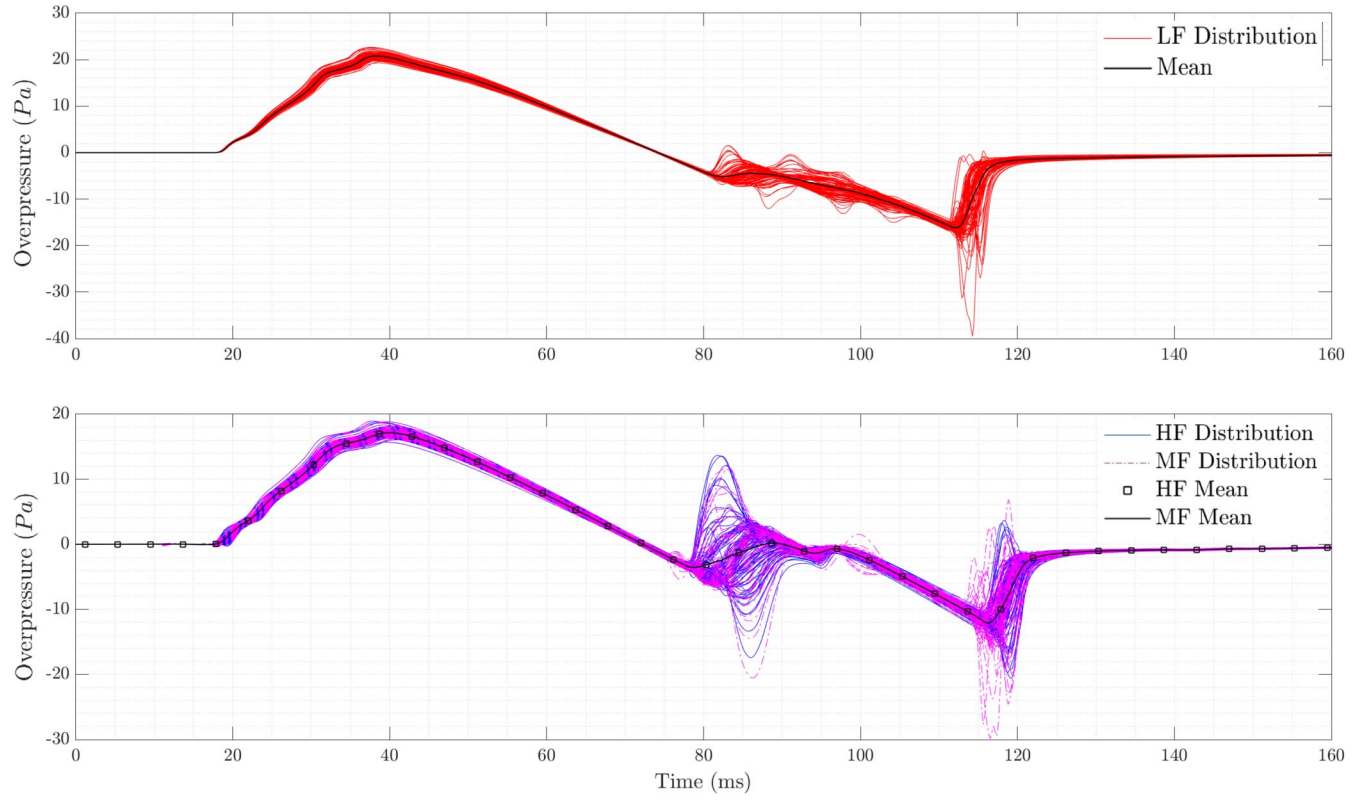

Fig. 18 Probable ground pressure signatures due to randomness.

completed in 49.24 s with a 2.3 GHz dual-core processor. As a consequence, probable ground pressure signatures acquired by using all surrogate models are compared in Fig. 18. This figure quantifies the possible peak overpressure values as well as their variations as intermediate responses. Likewise in the prediction of loudness level, MFPCE is able to predict both sequence of time and its corresponding sequence of overpressure values. The most notable aberration in overpressure value occurs around 120 ms.

IV. Conclusions

In this paper, we studied uncertainty quantification with multi-fidelity methods on both sonic boom loudness and ground pressure signature. Application is demonstrated on the JAXA Wing-Body aircraft from Second AIAA Sonic Boom Prediction Workshop. High-fidelity near-field pressure signature is obtained by employing the open-source SU2 suite. The Euler solver is chosen due to its relatively less computational expense when compared to viscous solvers. On the other hand, A502 PAN AIR, a supersonic potential flow solver, is integrated into the UQ framework as the low-fidelity flow solver. Attained near-field pressure is propagated throughout the atmosphere to the ground by using NASA's sBOOM, an aeroacoustic solver. Moreover, the angle of attack, Mach number, reflection factor, and ground elevation are chosen as random variables. The number of stochastic variables is restricted to 4 to avoid prohibitive computational cost.

Halton quasi-random sampling is conducted to obtain initial random variables to perform high- and low-fidelity analyses. One hundred forty low-fidelity and 70 high-fidelity sonic boom loudness and ground pressure signature computations are performed to obtain training and test datasets. Predetermined uncertainties are propagated through MFPCE and MFMC methods that are implemented as in-house Python codes in AeroMDO Laboratory. Additionally, for required surrogate models in MFPCE, error analyses are carried out up to the polynomial degree of 5 to observe best models in terms of prediction capability. In the application of MFMC, computational budget-related mean and variance estimations are presented. As scalar variable (i.e., ground loudness) estimations by multifidelity methods agreed with each other, we completed sequence estimation on the ground pressure signature data with only MFPCE. Similarly, resulting probable ground pressure signatures of the aircraft produced by proposed method is consistent with the high-fidelity PCE-based uncertainty quantification. Overall, the computational burden of the sonic boom uncertainty analysis is shrunk by half with the fusion of different fidelity levels in comparison with high-fidelity uncertainty analysis even though the entire data set is generated in advance. Thus, a further reduction in the computational cost may be achieved with the implementation of active learning techniques.

As concluding remarks, the most outstanding distinction between MFPCE and MFMC is that they embrace completely different approaches to obtain descriptive statistics of the uncertain response function. Multi-fidelity Polynomial Chaos Expansion (MFPCE) is a data-fusion method that uses an established Multi-fidelity (MF) surrogate model while performing sampling for the uncertainty quantification. MFMC, on the other hand, is a MF model-management method that does not construct a surrogate model. One of the other differences is the demanded computational sources by each of the methods such that, in the eight-dimensional computational application, MFMC swiftly estimates the mean and variance where MFPCE processes the data with a relatively higher computational cost. However, MFPCE excels at bringing in the distribution of the quantity of interest so higher-order statistics such as skewness and kurtosis could be attained in any application. On the other hand, MFMC is unable to produce probability distributions in conventional sense. MFPCE and MFMC yield results in a proximate time (i.e., the construction and prediction time) for the four-dimensional sonic boom case. However, this is not true for the eight-dimensional application. The efficiency of MFMC increases with the increase in the problem size, while the computational efficiency of the MFPCE method decreases. Moreover, it is experienced in the applications that MFMC requires substantially more low-fidelity analyses than MFPCE to reduce the variance. Hence, MFMC could be preferable whenever the low-fidelity simulation cost is significantly more affordable when compared to the high-fidelity simulation. At this point, in case of impeding low-fidelity simulation cost, a surrogate model that represents low-fidelity function may be obligatory to enlarge the low-fidelity data set. Additionally, these two methods behave similarly in some aspects as well. To illustrate, the number of high-fidelity analyses relies on the correlation between the high- and low-fidelity simulation results in both of the methods. The higher the correlation is, the less high-fidelity analyses are needed; thus, the more computationally efficient uncertainty quantification can be performed with either of the methods. In consequence, MFMC is advantageous whenever the problem is high-dimensional, the correlation between the low- and high-fidelity simulation is high, and the cost of the low-fidelity simulations is notably cheaper. Inversely, MFPCE is propitious in case of a considerable low-fidelity simulation cost and a low-dimensional space.

Acknowledgments

All authors would like to express their gratitude to TUBITAK for the research grant provided under the 218M471 TUBITAK 1001 project titled "Development of Multi-fidelity and Multidisciplinary Methodologies Integrating Sonic Boom, Aeroelasticity and Propulsion System for Supersonic Aircraft Design." The second and last authors would like to acknowledge the graduate thesis support provided by Istanbul Technical University Scientific Research Program for the MYL-2019-42352 project titled "Application of Multidisciplinary and Multi-fidelity Optimization Techniques for Supersonic Aircraft." The third and last authors would like to acknowledge the graduate thesis support provided by Istanbul Technical University Scientific Research Program for the MYL-2020-42758 project titled "Development of a Nonlinear Sonic Boom Prediction Program." The last author would like to acknowledge Istanbul Technical University Scientific Research Projects Unit for the "Stochastic Design Optimization of Military Sea and Air Vehicles" project with grant number MGA-2018-41090. The last author would like to thank NASA Langley Research Center for distributing the sBOOM sonic boom prediction code internationally for academic research.

References

[1] Phillips, B. D., and West, T. K., "Aeroelastic Uncertainty Quantification of a Low-Boom Aircraft Configuration," *2018 AIAA Aerospace Sciences Meeting*, AIAA Paper 2018-0333, 2018. https://doi.org/10.2514/6.2018-0333

[2] Nikbay, M., Stanford, B., West, T. K., and Rallabhandi, S. K., "Impact of Aeroelastic Uncertainties on Sonic Boom Signature of a Commercial Supersonic Transport Configuration," *55th AIAA Aerospace Sciences Meeting*, AIAA Paper 2017-0040, 2017. https://doi.org/10.2514/6.2017-0040

[3] West, T. K., and Phillips, B. D., "Multifidelity Uncertainty Quantification of a Commercial Supersonic Transport," *Journal of Aircraft*, Vol. 57, No. 3, 2020, pp. 491–500. https://doi.org/10.2514/1.c035496

[4] West, T. K., and Gumbert, C., "Multifidelity, Multidisciplinary Uncertainty Quantification with Non-Intrusive Polynomial Chaos," *58th AIAA/ASCE/AHS/ASC Structures, Structural Dynamics, and Materials Conference*, AIAA Paper 2017-1936, 2017. https://doi.org/10.2514/6.2017-1936

[5] Wang, F., Xiong, F., Chen, S., and Song, J., "Multi-Fidelity Uncertainty Propagation Using Polynomial Chaos and Gaussian Process Podeling," *Structural and Multidisciplinary Optimization*, Vol. 60, No. 4, 2019, pp. 1583–1604. https://doi.org/10.1007/s00158-019-02287-7

[6] Chaudhuri, A., Lam, R., and Willcox, K., "Multifidelity Uncertainty Propagation via Adaptive Surrogates in Coupled Multidisciplinary Systems," *AIAA Journal*, Vol. 56, No. 1, 2018, pp. 235–249. https://doi.org/10.2514/1.j055678

[7] Blonigan, P. J., Geraci, G., Rizzi, F., and Eldred, M. S., "Towards an Integrated and Efficient Framework for Leveraging Reduced Order Models for Multifidelity Uncertainty Quantification," *AIAA Scitech 2020 Forum*, AIAA Paper 2020-0420, 2020. https://doi.org/10.2514/6.2020-0420

[8] Ng, L. W.-T., Huynh, D. B. P., and Willcox, K., "Multifidelity Uncertainty Propagation for Optimization Under Uncertainty," *12th AIAA*

Aviation Technology, Integration, and Operations (ATIO) Conference and 14th AIAA/ISSMO Multidisciplinary Analysis and Optimization Conference, AIAA Paper 2012-5602, 2012. https://doi.org/10.2514/6.2012-5602

[9] Chaudhuri, A., and Willcox, K. E., "Multifidelity Uncertainty Propagation in Coupled Multidisciplinary Systems," *18th AIAA Non-Deterministic Approaches Conference*, AIAA Paper 2016-1442, 2016. https://doi.org/10.2514/6.2016-1442

[10] Quick, J., Hamlington, P. E., King, R., and Sprague, M. A., "Multifidelity Uncertainty Quantification with Applications in Wind Turbine Aerodynamics," *AIAA Scitech 2019 Forum*, AIAA Paper 2019-0542, 2019. https://doi.org/10.2514/6.2019-0542

[11] Peherstorfer, B., Willcox, K., and Gunzburger, M., "Optimal Model Management for Multifidelity Monte Carlo Estimation," *SIAM Journal on Scientific Computing*, Vol. 38, No. 5, 2016, pp. A3163–A3194. https://doi.org/10.1137/15m1046472

[12] Peherstorfer, B., "Multifidelity Monte Carlo Estimation with Adaptive Low-Fidelity Models," *SIAM/ASA Journal on Uncertainty Quantification*, Vol. 7, No. 2, 2019, pp. 579–603. https://doi.org/10.1137/17m1159208

[13] Peherstorfer, B., Beran, P. S., and Willcox, K. E., "Multifidelity Monte Carlo Estimation for Large-Scale Uncertainty Propagation," *2018 AIAA Non-Deterministic Approaches Conference*, AIAA Paper 2018-1660, 2018. https://doi.org/10.2514/6.2018-1660

[14] Ueno, A., Kanamori, M., and Makino, Y., "Multi-Fidelity Low-Boom Design Based on Near-Field Pressure Signature," *54th AIAA Aerospace Sciences Meeting*, AIAA Paper 2016-2033, 2016. https://doi.org/10.2514/6.2016-2033

[15] Carpenter, F. L., Cizmas, P., Bolander, C. R., Giblette, T. N., and Hunsaker, D. F., "A Multi-Fidelity Prediction of Aerodynamic and Sonic Boom Characteristics of the JAXA Wing Body," *AIAA Aviation 2019 Forum*, AIAA Paper 2019-3237, 2019. https://doi.org/10.2514/6.2019-3237

[16] Demiroglu, Y., Yildiz, S., and Nikbay, M., "Multi-Fidelity Sonic Boom Minimization of a Supersonic Aircraft by Parametric Wing Shape Design," *AIAA Scitech 2021 Forum*, AIAA Paper 2021-1009, 2021. https://doi.org/10.2514/6.2021-1009

[17] Choi, S., Alonso, J. J., and Kroo, I. M., "Two-Level Multifidelity Design Optimization Studies for Supersonic Jets," *Journal of Aircraft*, Vol. 46, No. 3, 2009, pp. 776–790. https://doi.org/10.2514/1.34362

[18] Economon, T. D., Palacios, F., Copeland, S. R., Lukaczyk, T. W., and Alonso, J. J., "SU2: An Open-Source Suite for Multiphysics Simulation and Design," *AIAA Journal*, Vol. 54, No. 3, 2016, pp. 828–846. https://doi.org/10.2514/1.j053813

[19] Carmichael, R., and Erickson, L., "PAN AIR—A Higher Order Panel Method for Predicting Subsonic or Supersonic Linear Potential Flows About Arbitrary Configurations," *14th Fluid and Plasma Dynamics Conference*, AIAA Paper 1981-1255, 1981. https://doi.org/10.2514/6.1981-1255.

[20] Giblette, T. N., and Hunsaker, D. F., "Prediction of Sonic Boom Loudness Using High-Order Panel Methods for the Near-Field Solution," *AIAA Scitech 2019 Forum*, AIAA Paper 2019-0605, 2019, pp. 1–11. https://doi.org/10.2514/6.2019-0605.

[21] Rallabhandi, S. K., "Advanced Sonic Boom Prediction Using the Augmented Burgers Equation," *Journal of Aircraft*, Vol. 48, No. 4, 2011, pp. 1245–1253. https://doi.org/10.2514/1.C031248

[22] Cleveland, R. O., "Propagation of Sonic Booms Through a Real, Stratified Atmosphere," Ph.D. Dissertation, Univ. of Texas at Austin, Austin, TX, 1995.

[23] Stevens, S. S., "Perceived Level of Noise by Mark VII and Decibels (E)," *Journal of the Acoustical Society of America*, Vol. 51, No. 2B, 1972, pp. 575–601. https://doi.org/10.1121/1.1912880

[24] Wiener, N., "The Homogeneous Chaos," *American Journal of Mathematics*, Vol. 60, No. 4, 1938, pp. 897–936. https://doi.org/10.2307/2371268

[25] Xiu, D., and Karniadakis, G. E., "The Wiener–Askey Polynomial Chaos for Stochastic Differential Equations," *SIAM Journal on Scientific Computing*, Vol. 24, No. 2, 2002, pp. 619–644. https://doi.org/10.1137/S1064827501387826

[26] Hosder, S., Walters, R., and Balch, M., "Efficient Sampling for Non-Intrusive Polynomial Chaos Applications with Multiple Uncertain Input Variables," *48th AIAA/ASME/ASCE/AHS/ASC Structures, Structural Dynamics, and Materials Conference*, AIAA Paper 20187-1939, 2007. https://doi.org/10.2514/6.2007-1939

[27] Ng, L. W.-T., and Eldred, M., "Multifidelity Uncertainty Quantification Using Non-Intrusive Polynomial Chaos and Stochastic Collocation," *53rd AIAA/ASME/ASCE/AHS/ASC Structures, Structural Dynamics and Materials Conference 20th AIAA/ASME/AHS Adaptive Structures Conference*, AIAA Paper 2012-1852, 2012. https://doi.org/10.2514/6.2012-1852

[28] Box, G. E. P., and Muller, M. E., "A Note on the Generation of Random Normal Deviates," *Annals of Mathematical Statistics*, Vol. 29, No. 2, 1958, pp. 610–611. https://doi.org/10.1214/aoms/1177706645

[29] Ng, L. W.-T., and Eldred, M., "Multifidelity Uncertainty Quantification Using Non-Intrusive Polynomial Chaos and Stochastic Collocation," *53rd AIAA/ASME/ASCE/AHS/ASC Structures, Structural Dynamics and Materials Conference*, AIAA Paper 2012-1852, 2012. https://doi.org/10.2514/6.2012-1852

[30] Halton, J. H., "On the Efficiency of Certain Quasi-Random Sequences of Points in Evaluating Multi-Dimensional Integrals," *Numerische Mathematik*, Vol. 2, No. 1, 1960, pp. 84–90. https://doi.org/10.1007/bf01386213

[31] Peherstorfer, B., Gunzburger, M., and Willcox, K., "Convergence Analysis of Multifidelity Monte Carlo Estimation," *Numerische Mathematik*, Vol. 139, No. 3, 2018, pp. 683–707. https://doi.org/10.1007/s00211-018-0945-7

[32] Ng, L. W. T., and Willcox, K. E., "Multifidelity Approaches for Optimization Under Uncertainty," *International Journal for Numerical Methods in Engineering*, Vol. 100, No. 10, 2014, pp. 746–772. https://doi.org/10.1002/nme.4761

[33] Palar, P. S., Tsuchiya, T., and Parks, G. T., "Multi-Fidelity Non-Intrusive Polynomial Chaos Based on Regression," *Computer Methods in Applied Mechanics and Engineering*, Vol. 305, June 2016, pp. 579–606. https://doi.org/10.1016/j.cma.2016.03.022

[34] Park, M. A., and Nemec, M., "Nearfield Summary and Statistical Analysis of the Second AIAA Sonic Boom Prediction Workshop," *Journal of Aircraft*, Vol. 56, No. 3, 2019, pp. 851–875. https://doi.org/10.2514/1.c034866

[35] Bolander, C. R., Hunsaker, D. F., Shen, H., and Carpenter, F. L., "Procedure for the Calculation of the Perceived Loudness of Sonic Booms," *AIAA Scitech 2019 Forum*, AIAA Paper 2019-2091, 2019. https://doi.org/10.2514/6.2019-2091

[36] West, T. K., Reuter, B. W., Walker, E. L., Kleb, B., and Park, M. A., "Uncertainty Quantification and Certification Prediction of Low-Boom Supersonic Aircraft Configurations," *Journal of Aircraft*, Vol. 54, No. 1, 2017, pp. 40–53. https://doi.org/10.2514/1.c033907